ARTICLE

Dynamics and Extensional Rheology of Polymer-Surfactant Association Complexes

Received 00th January 20xx,
Accepted 00th January 20xx

DOI: 10.1039/x0xx00000x

Carina D. V. Martínez Narváez, Thomas Mazur and Vivek Sharma*

Understanding and characterizing the influence of polymers and surfactants on rheology, application, and processing is critical for designing complex fluid formulations for enhanced oil recovery, pharmaceuticals, cosmetics, foods, inks, agricultural sprays, and coatings. It is well-established that the addition of anionic surfactant like sodium dodecyl sulfate (SDS) to an aqueous solution of an oppositely-charged or uncharged or polymer like poly(ethylene oxide) (PEO) can result in the formation of the polymer-surfactant association complexes (P^0S^-ACs) and a non-monotonic concentration-dependent variation in zero shear viscosity. However, the extensional rheology response of polymer-surfactant mixtures remains relatively poorly understood, partially due to characterization challenges that arise for low viscosity, low elasticity fluids, even though the response to strong extensional flows impacts drop formation and many processing operations. In this article, we use the recently developed dripping-onto-substrate (DoS) rheometry protocols to characterize the pinching dynamics and extensional rheology response of aqueous P^0S^- solutions formulated with PEO (P^0) and SDS (S^-), respectively. We find the PEO-SDS mixtures display a significantly weaker concentration-dependent variation in the extensional relaxation time, filament lifespan, and extensional viscosity values than anticipated by the measured shear viscosity.

Introduction

Macromolecular engineering of formulations requires understanding and characterization of the influence of macromolecular (polymers, proteins), condensed (particles, drops, bubbles), or self-associated (micelles and vesicles) dispersants on the interfacial and rheological properties.[1] Nearly a century of experimental and theoretical efforts have enabled us to elucidate how macroscopic shear rheology response of polymer solutions and melts depends on macromolecular properties, including the molecular weight, concentration, charge fraction as well as matrix/solvent properties.[1-5] However, the interaction and, often, the pairwise complexation of a polymer with another polymer, particle, surfactant, or micelle present significant challenges in formulation engineering, as the physicochemical hydrodynamics of various components, as well as the complexes, must be characterized and understood.[6-11] For example, in aqueous solutions, the interaction between polymers and surfactants can lead to spontaneous cooperative binding and complexation above a critical aggregation concentration (CAC), especially when one or both species are charged.[10, 11] In this contribution, we characterize and elucidate the influence of an uncharged polymer (P^0), an anionic surfactant (S^-), and their association complexes (PSACs or P^0S^-ACs) on the interfacial, rheological and processing behavior of model two-ingredient formulations. In previous studies,[8-14] for a fixed polymer concentration, an increase in shear viscosity as a function of surfactant concentration occurs beyond CAC, and a peak value manifests at the polymer saturation point (PSP), followed by a marginal decrease. However, it is unknown if similar non-monotonic trends arise for pinching dynamics and extensional rheology of P^0S^- systems, including P^0 = PEO (poly(ethylene oxide) and S^-=SDS (sodium dodecyl sulfate), motivating this study.

Polymer-surfactant mixtures and complexes influence the stability, rheology, and applications of paints and coatings, printing inks, cosmetics, foams, nanoemulsions, enhanced-oil recovery, agrochemical sprays, food, and biological fluids, such as saliva, and tracheal mucus.[8, 10, 15-21] Polymers perform the role of film or fiber formers, shear rheology modifiers, processing aids to change drop size distribution (in spraying and coating applications), or stickiness, and as stabilizers, flocculants, or compatibilizers. Surfactants change surface tension, alter wetting and spreading behavior, abet in foam and emulsion formation, solubilize drugs or dirt in micelles to facilitate drug delivery or detergency, and again as processing aids in free-surface flows. Spontaneous self-assembly of amphiphilic surfactants in aqueous solutions leads to the formation of micelles above a critical micelle concentration (CMC),[22] whereas in the presence of polymer, surfactants self-aggregate above CAC.[9, 10, 12, 23] In addition to shear viscosity, tensiometry, conductometry, NMR, and steady-state fluorescence quenching aid in identifying CMC and CAC.[9, 12-14, 24, 25] Several recent simulation papers attempt to provide a molecular picture of self-assembly and interactions.[26, 27] Though CAC < CMC, the CAC is lower by one order of magnitude or more if both species are oppositely charged leading strong electrostatic driving force. The two values are of a similar order for P^0S^- systems like PEO-SDS investigated here.

[a] 929 W. Taylor St, Chemical Engineering, University of Illinois at Chicago, IL. 60608
Electronic Supplementary Information (ESI) available: [details of any supplementary information available should be included here]. See DOI: 10.1039/x0xx00000x

Dispensing and liquid transfer to substrates by dripping, jetting, or spraying involve capillarity-driven pinching of liquid necks.[28-30] As streamwise velocity gradients associated with extensional flows arise in pinching necks, jettability, sprayability, spinnability, and stringiness depend on extensional rheology response and pinching dynamics.[28-30] Likewise, making foams and emulsions, gravure printing, and dispersal of drops by coughing, sneezing, and speaking, the underlying spread of viral flu involves pinching dynamics of multi-component fluids.[31-33] Addition of even a dilute amount of polymer with high molecular weight causes significant changes in the formation, size, and size distribution of drops.[17, 34-39] For Newtonian fluids, an interplay of viscous, inertial, and capillary stresses results in inertiocapllary, and viscocapillary dynamics respectively observed for low (*Oh* <1) and high viscosity Newtonian fluids (*Oh* >1). Here, the Ohnesorge number, $Oh = \eta/\sqrt{\rho\sigma R_0}$ provides a dimensionless measure of viscosity, (ratio of viscocapillary to inertiocapillary timescales), and scales the shear viscosity, with the square-root of the product of density, ρ surface tension, σ, and a length-scale, R_0.[28, 29] Polymer stretching and alignment in response to strong extensional flow fields within pinching necks contribute extra viscoelastic stresses that alter pinching rate and timespan.[34-41] Analysis of pinching dynamics allows characterization of the extensional relaxation time, λ_E and extensional viscosity, η_E. In solutions of flexible polymers like PEO,[42-48] λ_E can be much higher than the shear relaxation time, λ_s and η_E can be several orders of magnitude higher than shear viscosity, η_s, though Newtonian fluids exhibit a Trouton ratio, $Tr = \eta_E/\eta_s = 3$ (and thus, one parameter captures their flow behavior).

However, characterizing extensional rheology response is rather challenging as measurements require bespoke instrumentation, display high sensitivity to deformation history, and can be influenced by elastic or inertial flow instabilities that can arise in microfluidic and stagnation flow devices.[29, 37, 49-54] Furthermore, most techniques are suited for fluids with relatively high viscosity, and typically the range of accessible strain or strain rates is rather limited.[37, 44, 47, 50, 51, 55] Table 1 summarizes the published datasets[56-63] on P^0S^- systems made with two commercially-available techniques: RFX opposed jet and CaBER (capillary breakup extensional rheometer). The measurements rely on a flexible, relatively high molecular weight (M_w) polymer, and the few data points included show that the critical extensional rate, $\dot{\varepsilon}_c$ beyond which strain hardening appears, decreases on surfactant addition. The range (and number) of surfactant concentrations explored at a fixed polymer concentration is limited, and it is not apparent if the extensional rheology response exhibits a non-monotonic concentration-dependent variation. Furthermore, Dontula *et al.* showed that strong inertial and shear within the nozzle effects render the opposed jets technique unsuitable for quantitative or accurate measurements of η_E.[60, 64] Likewise, characterization with standard capillary breakup extensional rheometer (CaBER) protocols is limited to liquids with λ_s, $\lambda_E > 1$ ms and $\eta_s > 50$ mPa · s, as a finite time (nearly 50 ms) is needed for applying step-strain to a liquid bridge formed between two plates.[29, 51, 65] Indeed, Miller and Copper-White[62] note: "These solutions are at the very threshold of the operational space for the CaBER technique." The motivations underlying the current contribution are three-fold: (i) address the characterization challenges using dripping-onto-substrate (DoS) rheometry protocols we developed recently, [44-48, 53, 66-69] (ii) obtain comprehensive datasets to examine non-monotonic concentration-dependence is observed in processes influenced by pinching dynamics and extensional rheology response, and (iii) seek an understanding of the role played by a combination of electrostatic and hydrodynamic stretching for uncharged polymer (P^0), an anionic surfactant (S^-), and their association complexes (PSACs or P^0S^-ACs).

Table 1. The response of uncharged polymer – ionic surfactant solutions to extensional flows: summary.

Authors, Reference (Year)	Polymer-Surfactant (M_w g/mol), Solvent	$c_{polymer}$ (wt.%) $c_{surfactant}$ (mM)	Technique	Remarks
Eastman, Goodwin & Howe[56] (2000)	PVP-SDS (0.7x10^6)	$c > c^*$ 27-500 mM	RFX Opposed-jet	Strain hardening observed
Smitter… Saez[57-59] (2001-2002)	PEO-SDS (4x10^6 & 8x10^6)	0.01< c / c^* < 2 c < CMC	RFX Opposed-jet	$\Delta P\ vs.\ \dot{\varepsilon}$ plots show strain hardening, $\dot{\varepsilon}_c$ decreases on adding SDS
Cooper-White, et al.[60] (2002)	PEO-SDS (1x10^6) 50 wt.% glycerol	c / c^* ~1 ; 8-32 mM	RFX Opposed-jet	Tr <120, Strain hardening, $\dot{\varepsilon}_c$ decreases on adding SDS
Torres... Saez[61] (2008)	PEO-SDS or SDBS (4x10^6)	500 ppm c < c*=550 ppm	RFX Opposed-jet	Extensional thickening. $\dot{\varepsilon}_c$ decreases above CAC.
E. Miller & Cooper-White[62] (2009)	PEO-SDS (2x10^6)	0.75 wt.% 5, 8, 16, 32 mM	CaBER	$\lambda_E$and apparent η_E reported for four SDS concentrations
Wang... Cooper-White[63] (2016)	PEO-Tween20 or SDS (2x10^6)	0.75 wt.% c / c^* < 1	CaBER	λ_E reported. DST measurements included.

Experimental Methods and Materials

We characterize the pinching dynamics and extensional rheology response using dripping-onto-substrate (DoS) rheometry protocols.[44-48, 53, 66, 67] Several studies, including our own, describe the characterization of the extensional rheology and pinching dynamics using (DoS) rheometry for solutions of neutral and charged polymers,[44-47, 53, 66, 67, 70-78] inks and particle suspensions,[46, 79, 80] wormlike micellar solutions,[46, 81-84] hydrocolloids and food materials (cellulose gum solutions, ketchup, mayo),[46, 67] and cosmetics (nail lacquer formulations, hand-cream, shampoo, and conditioners).[46, 68, 69] The DoS rheometry involve visualization and analysis of pinching necks created by dripping a finite volume of a liquid from a fixed nozzle onto a partially wetting substrate. Briefly, the fluid is pumped at a low and fixed flowrate, Q = 0.02 mL/min through a nozzle with an outer and inner diameter of $D_0 = 2R_0 = 1.27$ mm and $D_i = 0.838$ mm, respectively. A finite volume of the liquid is released onto a substrate placed at distance *H*, such that the aspect ratio of H / D_0 ≈ 3. The DoS videos are further analyzed with specially written MATLAB codes for determining radius evolution over time. We measure the surface tension values using the maximum bubble pressure tensiometry (MBPT) set-up we built. MBPT relies on the measurement of maximum bubble pressure as a function of bubbling rate and facilitates the measurement of time-dependent variation in surface tension correlated with the rate of mass transfer of surface-active agents to a freshly formed interface.[85-87] We checked that the pseudo-equilibrium values obtained using MBPT are comparable to equilibrium surface tension values obtained using pendant drop tensiometry and identify CMC and CAC values. We report steady shear viscosity measurements made using a torsional rheometer, using a concentric cylinder (double gap) Couette cell on an Anton Paar MCR 302 rheometer at 25 °C.

The polymer PEO with an average molecular weight M_w = 1.0 × 10^6 g/mol and the surfactant SDS purchased from Sigma-Aldrich were used without further purification. Aqueous PEO solutions were prepared by slowly adding dry polymer powder to deionized water. The PEO solutions were left on a roller for a minimum of five days to ensure homogeneous and slow mixing, as high shear mixing flows can lead to chain scission.[88, 89] Subsequently, SDS was added and left overnight on a roller for complete mixing. The polymer concentrations used in this study lie below the overlap concentration (c^* = 0.17%) of the surfactant-free polymer solutions. The stretching of PEO chains by electrostatics on complexation with charged surfactant and micelles, and by hydrodynamics in extensional flows lower threshold for overlap and interchain interactions.[2, 4, 42, 47, 48, 66, 90]

Results and discussion

Critical aggregation concentration (CAC) and polymer saturation point (PSP)

Figure 1a shows that the surface tension of the polymer-free solutions progressively decreases with c_{SDS} but attains a relatively constant value above a CMC. For a fixed PEO concentration, SDS addition lowers the surface tension up to CAC that signals the onset of the polymer-surfactant complexation. Beyond polymer saturation point (PSP), surface tension decreases towards the values for polymer-free SDS solutions. The plot of specific viscosity $\eta_{sp} = (\eta_0 - \eta_s)/\eta_s$ as a function of c_{SDS} (see Figure 1b) displays a plateau region at low surfactant concentration, and an increase in viscosity above the critical aggregate concentration (CAC), with the peak value at PSP. At excess micelle point (EMP), the unimer concentration equals the CMC value, and free micelles form. Here viscosity of water defines solvent viscosity, η_s , such that η_{sp} values capture the solute contribution to η_0. Specific viscosity measured at lower polymer concentrations (0.08 and 0.01 wt.%) exhibits the same CAC value of 5 mM. However, the PSP value depends on polymer concentration, in agreement with the previous reports on P^0S^- systems including PEO-SDS, PEO-SBDS, and PVP-SDS.[61, 91] The changes in surface tension and steady shear viscosity are influenced by the surfactant-like and the polymer-like behavior of the polymer-surfactant complex, respectively.[25]

Figure 1c schematically illustrates the evolution of uncharged polymer – anionic surfactant (P^0S^-) interactions and complexation under equilibrium conditions as a function of surfactant concentration. The picture, inspired by previous experimental and theoretical work, is sketched for a dilute polymer concentration.[8-14, 24, 92-95] The onset of P^0S^- complexation occurs at CAC as self-assembly drives the formation of surfactant clusters or "beads" (bound micelles) on stringlike polymer chains, forming a "beaded-necklace."[9, 10, 96] The colored background in Figure 2 visually aids in identifying the four regimes: I: Below CAC; both polymer and surfactant unimers coexist in equilibrium: no bound or free micelles, no necklace. II: CAC-PSP, the formation of partially beaded-necklace, and coil expansion. III PSP-EMP, the size and number of beads increases with $c_{SDS.}$ IV: EMP – beyond, beaded necklace, free micelles, and unimers coexist. The increase in c_{SDS} beyond PSP leads to increased electrostatic screening and coil contraction. As free micelles form above EMP, it is also referred to as CMC_p. The size of beads or the aggregation number, N_{agg} (20-50) for SDS clusters bound to PEO at c_{SDS} << PSP is lower than the N_{agg} = 60-80 for free micelles in the polymer-free SDS solutions (c_{SDS} <100 mM).[97, 98] The N_{agg} increases with c_{SDS} in both cases, and above PSP, beads have N_{agg} similar to free micelles.[92, 98] The beaded-necklace chain in the presence of excess unimers is hydrodynamically similar to a polyelectrolyte chain in the presence of added ions.[25]

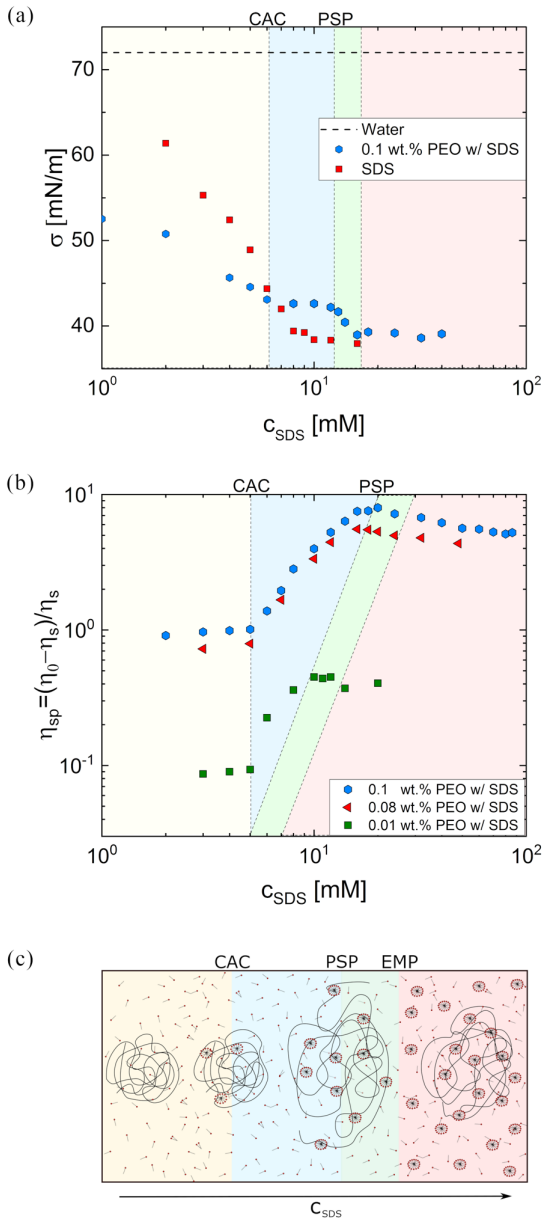

Figure 1. Surface tension and specific viscosity of SDS/PEO solutions. a) Surface tension of SDS solutions and 0.1 wt.% PEO as a function of SDS concentration. CAC (6 mM) is lower than CMC (8.2 mM). Surface tension values exhibit a mild decrease above CAC. At regime IV, values approach the free-polymer SDS curve (red). (b) The specific viscosity of SDS/PEO as a function of c_{SDS} shows distinct regimes delimited by the critical aggregation concentration (CAC) at 5 mM SDS, and the polymer saturation concentration (PSP) that depends on polymer concentration. PEO concentration corresponds to a dilute regime in surfactant-free solutions. The two dotted lines that show PSP and excess micelle point, EMP respectively are included in (a) as well. The PSP (12.5 mM) and EMP (18 mM) for 0.1 wt. % values shift to lower concentrations for 0.08 wt.% and 0.01 wt.% PEO. (c) Schematic shows conformation of the polymer-surfactant association complex as a function of anionic surfactant concentration for a fixed amount of an uncharged polymer.

Characterization of pinching dynamics

We use DoS rheometry protocols to investigate the influence of change in conformation of beaded-necklace chains on pinching dynamics and extensional rheology response. In a typical DoS rheometry experiment, drops are released onto an unbounded, partial wetting substrate at distance *H* from the nozzle of diameter $2R_0$. However, as surfactants can influence wettability,[99, 100] here we evaluate the influence of partial vs pinned wetting, before discussing the extensional rheology response. Figure 2a shows the pendant drops visualized before touching and spreading for both partial and pinned wetting, and includes a schematic illustrating how a disc-shaped substrate provides a pinned contact line. Figure 2b shows the sessile drop diameter expansion for 24 and 40 mM SDS with 0.1 wt.% PEO over the partially wetting substrate. An initial scaling of $t^{1/7}$ associated spreading involving dissipation near the contact line,[100] observed for both concentrations followed by a plateau regime that coincides with the elastocapillary region (EC), relevant for extensional rheology characterization (discussed next). The apparent contact angle and the diameter of the sessile drop are nearly unchanged between the instants 1 and 2 (see snapshots), and further spreading occurs long after pinch-off event (image at instant 3 is at t = O(1000 ms), whereas pinch-off occurs before t <50 ms).

The neck shape evolution for pinned and partial wetting conditions are included in Figure 2c for 20 and 40 mM SDS with 0.1 wt.% PEO, and visually, the neck shape and pinching rate appear comparable. The corresponding radius evolution data included in Figure 2d shows that partial and pinned wetting display quantitatively similar behavior. We include an additional dataset for 10 mM SDS to highlight the similarity in the neck thinning dynamics. In our studies with DoS rheometry protocols, the pinching laws used are derived for self-thinning dynamics by assuming that spreading and pinching dynamics are decoupled.[44-48, 53] Though in Dinic *et al.*[46] we discussed the use of a pinning contact line on a disk to emulate a pinned lower drop in CaBER experiments, we found partial wetting substrates provide pragmatic and quantitative measurements. Our choice was also guided by our experimental observations using different substrates consonant with the extensive literature on the influence of moving contact lines on the capillary breakup, and transfer ratio (TR: the fraction of liquid transferred to a lower plate) that find an enhancement in pinching rates and TR on wetting substrates (relatively small contact angles, and high surface energy). [101-106] Previously, Zhang and Muller[81] utilized the pinned wetting for DoS rheometry of surfactant solutions. More recently, Wu et al.[84] dripped wormlike micellar solutions on high surface energy metal surfaces, and found that the moving contact lines impact pinching dynamics only for Capillary number, Ca >0.1, where $Ca = \frac{\eta U}{2\gamma}\cos\theta$ is defined using mean spreading velocity, U and apparent contact angle, θ. We find Ca << 0.1 for partial wetting substrates (larger θ, leads to smaller Ca). In practice, the wetting behavior of substrate must be evaluated for each liquid used in DoS rheometry experiments.

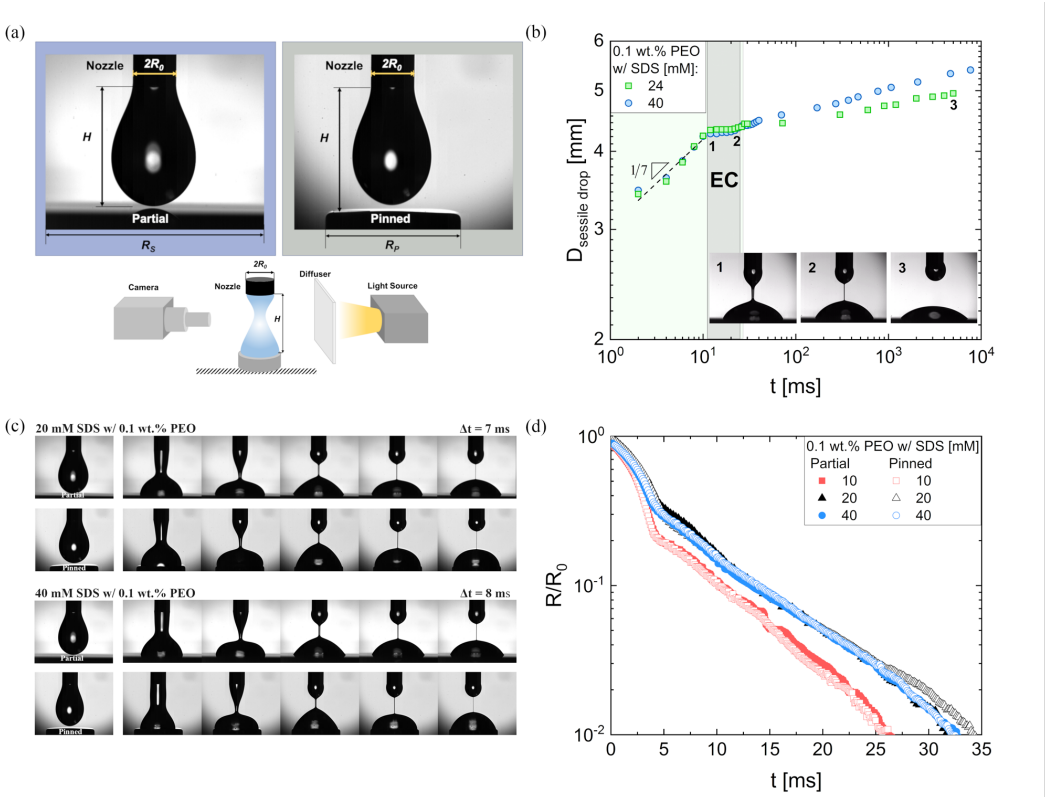

Figure 2. Contrasting pinching dynamics and dripping-onto-substrate (DoS) experiments using a partial vs a pinned wetting substrate. (a) Zoomed-in images of the pendant drops formed using dripping-onto-substrate protocols right before a contact with a partial (left) or pinned (right) substrate placed at a distance, H from the nozzle of diameter $2R_0$ such that $H/2R_0 \approx 3$. Dripping-onto-substrate setup includes a high-speed camera and a light source with a diffuser. A dispensing system (not shown) includes a syringe pump connected to a nozzle ($2R_0$) and is used to release a finite fluid volume onto a partial or pinned wetting substrate. A disc of diameter $2R_P$ is used to pin the contact line. (b) Evolution of the sessile drop diameter as a function of time tracked on a partial wetting substrate for two PEO/SDS solutions. Drop spreading exhibits an initial growth law of $t^{1/7}$ as shown for both 24 and 40 mM SDS dissolved in aqueous solution of 0.1 wt.% PEO. The spreading rate is quite low in EC regime and after pinch-off. Three snapshots are included to visualize the change in the relative drop size. (c) Image sequences show changes in neck shape and sessile drop size on partial wetting and pinned substrates. No significant changes can be perceived during the pinching process. The time step between snapshots for 20 mM SDS and 40 mM formulated in aqueous PEO (0.1 wt.%) solution is 7 and 8 ms, respectively. (d) Neck radius evolution compared for three SDS concentrations in 0.1 wt.% PEO solution using a partial wetting (closed symbols) and a pinned substrate (empty symbols). Nearly matched response is observed.

Figure 3a shows the neck shape evolution of PEO/SDS mixtures with a matched starting point of $R/R_0 \sim 0.5$. A single conical neck forms for pure water as shown in the image sequence in the top row with a timestep, $\Delta t = 0.5$ ms. In contrast, slender cylindrical necks form for the polymer-surfactant solutions and exhibit delayed pinch-off ($\Delta t = 5$ ms). An increase in SDS concentration leads to a non-monotonic change in filament lifespan, t_f thus requiring more snapshots for 16 mM SDS than for 8 mM as well as 32 mM SDS. Interaction of PEO with the ionic surfactant, SDS leading to the formation of an electrostatically stretched beaded-necklace increases t_f and $\eta_0(c_{\mathrm{SDS}})$, and shifts the onset of shear thinning response for c_{SDS} >8 mM to the measurable range, as seen in Figure 3b (the Carreau model fits are included as a dotted line).

Though the addition of 12 mM and 60 mM SDS to the PEO solutions results in a nearly matched shear viscosity, the pinching dynamics are remarkably dissimilar, with a longer pinching time manifested for 60 mM. The radius evolution data in Figure 3c also displays a longer t_f for 16 mM than for 32 mM, and though t_f for 60 mM is larger than for 32 mM. As the shear viscosity of the P^0S^- systems used in the study is relatively low, leading to Oh < 1, the initial radius evolution shows an inertiocapillary response for all mixtures, described by the following expression:

$$\frac{R}{R_0} = X\left(\frac{t_p - t}{t_R}\right)^{2/3} \qquad (1)$$

Here the inertiocapillary or Rayleigh time, $t_R = \sqrt{\rho R^3/\sigma}$ and t_p represents the pinch-off time or filament lifespan for a Newtonian fluid and is a parameter for fitting the IC regime for polymeric fluids. The experimentally measured values of X as well as the values obtained using volume-of-fluid based numerical simulations vary between 0.4-0.6, as detailed elsewhere.[28, 29, 107] Even though the interplay of gravity and capillarity influences the shape of the pendant drop, gravity exercises a

negligible impact on the pinching dynamics. The value of the dimensionless group, Bond number, $Bo = \Delta\rho g R^2/\sigma$ becomes rather small as pinching proceeds for it ranges between Bo = 0.06-0.1 if nozzle size $R = R_0$, is used for estimation, and Bo<<1 within the pinching neck.

In contrast, the second elastocapillary regime displays an exponentially slow decay in the radius that can be described by the following expression:

$$\frac{R(t)}{R_0} = \left(\frac{G_E R_0}{2\sigma}\right)^{1/3} \exp\left(-\frac{t-t_c}{3\lambda_E}\right) \quad (2)$$

The simplest expression for elastocapillary response based on the Oldroyd-B model[40, 90, 108-113] uses shear modulus and shear relaxation time as parameters. However, the measured extensional relaxation time, λ_E usually differs in magnitude and concentration-dependent variation from the shear relaxation time for flexible polymers like PEO due to the role of stretched chain hydrodynamics. Likewise, the apparent extensional modulus, G_E which can be computed from the neck radius at the transition from IC to the EC regime at t_c, also exhibits values distinct from shear modulus. The measured differences arise due to the influence of chain stretching, conformation-dependent drag, and finite extensibility, and for flexible polymers, strong extensional flows can lead to coil-stretch transition.[47, 48, 53, 114-116] The EC fits to the radius evolution data are shown as a dotted line in Figure 3c.

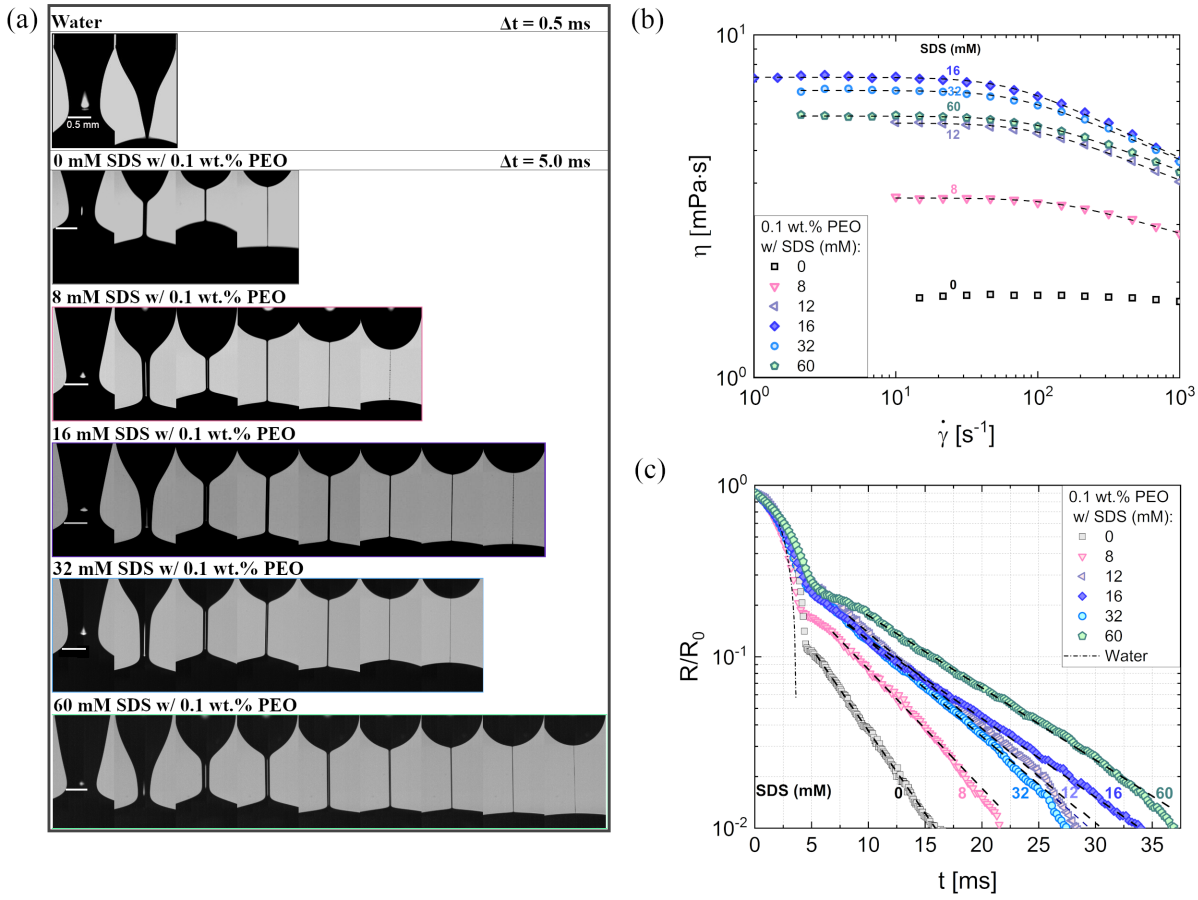

Figure 3. Contrasting the concentration dependence on radius evolution data obtained using DoS rheometry and shear viscosity data obtained with torsional rheometry. (a) Representative snapshots exhibit a comparison of different neck shapes for water, polymer (PEO), and polymer-surfactant solutions (PEO/SDS). (a) The shear rheology response of polyethylene oxide (PEO) and sodium dodecyl sulfate (SDS) aqueous solutions were characterized using a concentric cylinder (double gap) Couette cell on an Anton Paar MCR 302 rheometer at 25 °C. A matched flow curve is observed for 12 and 60 mM SDS. The Carreau model fits are included as a dotted line. (c) Radius evolution of PEO/SDS solutions. The addition of SDS to polymer solutions (PEO) delays pinch-off event compared to the polymer solution with no SDS added. 60 mM SDS do not overlap with 12 mM, as seen in shear viscosity data. Dashed lines show EC fits obtained using equation (2).

In some cases, finite extensibility effects,[47, 48, 53, 117, 118] (not included in the Oldroyd-B model) manifest as a terminal viscoelastocapillary (TVEC) regime, with a linear decrease in radius $R(t)/R_0 = (t_f - t)/t_{TVEC}$. Here $t_{TVEC} = 2OhTr^{\infty}$ with $Tr^{\infty} = \eta_E^{\infty}/\eta$ defined as the ratio of a strain-rate and strain independent steady, terminal extensional viscosity, η_E^{∞} and the rate-independent zero shear viscosity. The fits to the TVEC regime allow the computation of η_E^{∞} and the filament lifespan, t_f (or the overall pinch-off time). Table 2 lists the parameters extracted by analyzing the radius evolution data and also includes the values of the zero shear viscosity and surface

tension measured using torsional shear rheometry and maximum bubble pressure tensiometry.

Extensional relaxation time and extensional viscosity

Figure 4a shows the plot of G_E and t_c *vs.* c_{SDS} and even though the value of t_c shows slight variation, G_E increases linearly up to PSP here error bars are similar to the size of symbols). Figure 4b shows that the extensional relaxation time, λ_E obtained by fitting the radius evolution profiles included in Figure 3c (and the data for a few extra concentrations) for a fixed PEO (0.1 wt.%) concentration, exhibits a non-monotonic variation with c_{SDS}. The peak observed at 14 mM exhibits λ_E value that is 2.3 times the value obtained for the surfactant-free PEO solution (included as a horizontal line). As the c_{SDS} increases, λ_E remains nearly constant even as CAC is exceeded, and λ_E increases with concentration once c_{SDS} exceeds 10 mM (~ 2 times CAC), rising to a peak value at 14 mM even though PSP = 20 mM is computed from the specific viscosity curve. We observe that the filament lifespan, t_f also exhibits a non-monotonic concentration dependence distinct from the response expected using shear rheology response. On increasing surfactant concentration further, λ_E value dips and then increases again beyond c_{SDS} = 24 mM. In addition to extensional relaxation time, the analysis of radius evolution data using the expression $\eta_E\dot{\varepsilon}(t)=\sigma/R(t)$ facilitates the computation of an apparent extensional viscosity $\eta_E=\eta_E^t(\varepsilon,\dot{\varepsilon},t)$. The balance between extensional and capillary stresses is carried out assuming inertial and viscous terms are negligible. Here, capillary stress depends on the ratio of surface tension, σ to the transient neck radius. Though the effect of dynamic adsorption is not considered here (a detailed investigation is ongoing), previous studies indicate that soluble surfactants with fast adsorption kinetics and concentrations above CMC show significant surface coverage,[119-122] unlike insoluble surfactants that provide contributions by Marangoni stresses and are entirely swept away from the pinch-off zone in the late stage.[123, 124] The extension rate, $\dot{\varepsilon}=-2\dot{R}(t)/R(t)$ determined from the radius evolution profiles, exhibits a constant value in the EC regime. However, in IC and TVEC regimes, the value diverges as $\dot{\varepsilon}=2n/(t_p-t)$ with n = 2/3 and 1 respectively.

The apparent extensional viscosity plotted as a function of Hencky strain, $\varepsilon=2\ln\left(R_0/R(t)\right)$ in Figure 4c exhibits strain hardening for all systems and the TVEC regime is manifested for the solutions with c_{SDS} >24 mM. The extensional viscosity value and Tr for the surfactant-free PEO solution are higher than the PEO-SDS solutions with c_{SDS} <16 mM. The measured value of maximum extensional viscosity that correspond to the steady, terminal extensional viscosity values for c_{SDS} > 24 mM, shown in the inset of Figure 4c, show relatively weak concentration-dependent variation in comparison to the shear viscosity response. The Tr ratio estimated using the ratio of these plotted values to the corresponding zero shear viscosity values are nearly three times lower than the value measured for the SDS-free PEO solution, correlated with the higher extensibility (ratio of stretched chain to unperturbed coil size) in comparison to electrostatically stretched, beaded-necklace chains. The Trouton ratios measured for PEO-SDS solutions are in the range of $Tr\sim O(10^3-10^4)$, that is up to two orders of magnitude greater than the values calculated using the opposed-jet technique and reported by Cooper-White et al.[60] for similar PEO-SDS solutions (made with glycerol-water mixtures and 0.15 wt. % PEO). However, $Tr\sim O(10^3-10^4)$ agree with the more recent extensional viscosity values measured using CaBER (for SDS < 32mM) by the same co-authors.[62, 63] However, as the opposed-jet technique presents challenges for quantitative characterization,[60, 64] and both capillarity-based methods show comparable Tr values, we conclude that even though the maximum extensional viscosity is 10^3-10^4 fold higher, the nearly-matched stretched chain size provides comparable values for the PEO-SDS solutions as shown in the inset of Figure 4c.

A comparison of the shear and extensional relaxation times is shown in Figure 4d. Remarkably, the λ_s values estimated using the Carreau model fits for 12-60 mM are an order of magnitude larger than the λ_E values, implying that the conformations, strain, degree of chain overlap, and relaxation dynamics are quite different in shear and extensional flow fields. Though extensional relaxation time is longer than λ_s for neutral polymers as well as polyelectrolytes,[37, 38, 42, 45, 47, 48, 66, 67, 71, 90] the rather large values for λ_s observed in the polymer-surfactant mixtures compared to extensional relaxation time are consistent with three scenarios. Previous studies that show $\lambda_s>\lambda_E$ arises due to the role played by transient junctions created by entanglements for neutral polymers,[43, 125] and by stickers for associative polymer solutions.[126] The observation of $\lambda_s>\lambda_E$ in wormlike micellar fluids[127-130] is often attributed to different dynamics of micelle creation and destruction for the stretched states in response to shear and extensional flow. Here, the PEO concentration is relatively low compared to entanglement concentration and SDS concentrations are well below the range where wormlike micelles form. Even though complexation expands coils and alters the size of self-assembled structures, the formation of entanglements or wormlike micelles is unlikely. Therefore, the observation of $\lambda_s>\lambda_E$ suggests that some beads are acting as transient junctions, and the creation and destruction rate of such junctions change in the presence of strong extensional flows.

Table 2. Concentration-dependent parameters of zero shear viscosity, shear relaxation time, surface tension, transition time, the scaled radius at the onset of EC regime, filament lifespan, and extensional relaxation time are extracted from the radius evolution data for 0.1 wt.% PEO solution with a range of SDS concentrations.

c_{SDS} (mM)	η_0 (mPa · s)	λ_S (ms)	σ (mN m^{-1})	t_c (ms)	R_c/R_0 (-)	t_f (ms)	λ_E (ms)
0	1.7	-	62.1	4.6 ±0.1	0.112	13.9 ±0.3	1.5 ±0.05
2	1.7	-	48.2	4.7 ±0.2	0.101	19.5 ±0.2	2.1 ±0.04
4	1.8	-	45.4	4.5 ±0.1	0.136	17.7 ±0.3	2.0 ±0.01
5	1.8	-	44.6	5.1 ±0.2	0.143	19.0 ±0.7	1.9 ±0.06
8	3.4	7.3	43.3	4.7 ±0.4	0.167	20.0 ±0.6	2.1 ±0.01
10	4.4	8.0	43.0	4.5 ±0.4	0.205	20.4 ±1.6	2.2 ±0.04
12	5.6	10.8	42.2	4.2 ±0.5	0.302	26.5 ±0.8	2.6 ±0.03
14	6.5	11.8	40.3	5.0 ±0.2	0.227	28.1 ±1.4	3.4 ±0.04
20	8.0	14.1	39.8	5.1 ±0.2	0.270	29.2 ±0.9	2.9 ±0.07
24	7.3	12.6	39.1	4.7 ±0.2	0.281	26.1 ±0.5	2.5 ±0.04
32	6.9	13.4	38.6	4.9 ±0.5	0.246	25.2 ±0.7	2.6 ±0.01
40	6.4	12.0	39.0	5.9 ±0.5	0.246	29.5 ±1.4	3.4 ±0.13

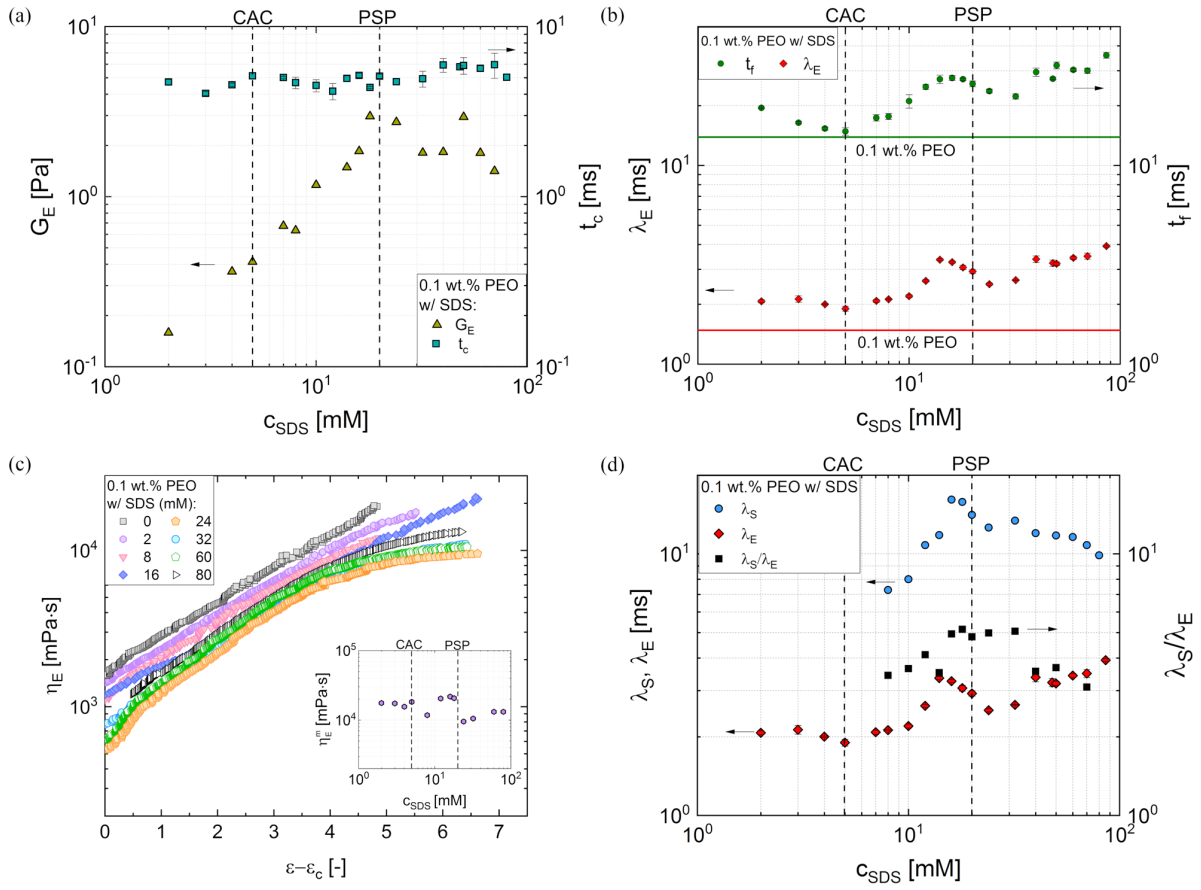

Figure 4. Extensional rheology response of aqueous solution of polymer-surfactant mixtures (0.1 wt.% PEO with variable c_{SDS}). (a) Apparent extensional modulus and transition time as a function of c_{SDS}. (b) Extensional relaxation time and filament lifespan of the PEO/SDS solutions. Horizontal lines represent the measured parameters for a PEO solution with no added surfactant. (c) Extensional viscosity as a function of Hencky strain and the inset shows the maximum value measured as a function of c_{SDS}. (d) Extensional and shear relaxation times of the PEO/SDS solutions show values that differ significantly, and the peak values also occur at distinct concentrations. The shear relaxation time λ_s is nearly an order of magnitude larger than λ_E.

ARTICLE

Figure 5 summarizes the key findings of this contribution and presents the contrasting shear and extensional rheology response using zero shear viscosity and extensional relaxation time values obtained for the aqueous PEO-SDS mixtures normalized by the corresponding values obtained for SDS-free PEO solutions with 0.08 wt.% and 1 wt.% PEO. Though shear viscosity increases by nearly an order of magnitude, the extensional relaxation time increases only by a factor of two, and the peak values for the latter are not obtained at the PSP or the peak observed in shear viscosity measurements. The increase in concentration-dependent zero shear rate viscosity η_0 values at low c_{SDS}, up to a peak at PSP, followed by a dip is often attributed to the influence of surfactant unimers and bound/free micelles on the conformation of "beaded-necklace" polymer chains. The range and extent of electrostatic interactions affect polymer conformation and influence inter- and intrachain interactions that lead to nearly an order of magnitude higher peak viscosity. A ten-fold increase in viscosity implies the beaded necklace chains are either in semi-dilute regime (as the overlap concentration for polyelectrolytes is lower, and semi-dilute regime that arises for c^*>1 shows $\eta_{sp} > 1$) or the beads effectively behave like transient junctions (complexes behave like associative polymers).

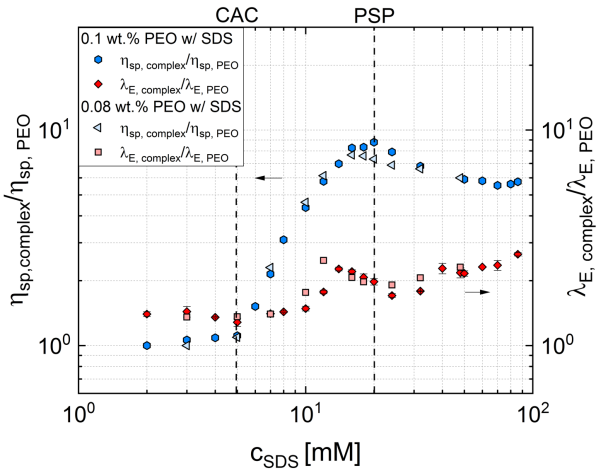

Figure 5. Comparison of extensional and shear rheology response of aqueous solution of polymer-surfactant mixtures (0.1 wt.% PEO with variable c_{SDS}). Normalized specific viscosity contrasted with normalized extensional relaxation time shown for solutions formulated with 0.1 wt.% and 0.08 wt.% PEO. Critical aggregation concentration (CAC) and polymer saturation point (PSP) observed in shear viscosity measurements (showed in dotted lines) do not capture the transition concentrations for concentration-dependent variation of extensional rheology response.

The solution viscosity is relatively low and hence the viscoelastic response is below the resolution in the oscillatory shear measurements, thus preventing us from making direct comparisons with transient network models. However, the onset of shear thinning and the decay constant obtained from elastocapillary pinching provide us with two distinct measurements of relaxation time, contrasted in Figure 4d. The enhanced values of η_0 and λ_s, and limited or complete disassociation of such transient junctions in strong flows,[126] leading to shear thinning response as well as manifestation of extensional relaxation time, λ_E values comparable to the stretched neutral chains. Extensional rheology characterization of multi-sticker associative polysaccharides with flow birefringence and excess pressure drop across a stagnation point in cross-slot extensional rheometer[37] and of hydrophobically modified alkali-soluble emulsion (HASE) polymers using opposed jets[131] suggest that associative polymer solutions show a pronounced degree of extensional thinning as the response is dictated by destruction of the transient network. In contrast, the aqueous solutions of PEO-SDS mixtures show strain hardening in Figure 4c, with nearly matched maximum extensional viscosity values. However, the studies on associative polysaccharides were carried out at much higher polymer volume fractions and as polysaccharides show lower flexibility and extensibility than PEO, the relatively enhancements in Tr ratio even for bare polysaccharides are quite low at comparable molecular weights.[47, 48, 53]

Conclusions

In summary, the addition of SDS to an uncharged polymer like PEO increases the pervaded volume, leading to a lower overlap concentration, lower critical shear rate for the onset of shear thinning, and higher measured specific viscosity values (almost an order of magnitude higher). However, the extensional relaxation time and extensional viscosity exhibit a weaker concentration-dependence as the relaxation dynamics and drag of the hydrodynamically-stretched chains are comparable even if surfactant changes the equilibrium coil size. The relatively weak variation in filament lifespan and extensional relaxation time cannot be anticipated with shear rheology characterization. We rationalize the observations by treating P^0S^-ACs as stretched, charged, beaded-necklace chains with electrostatic-stretching determined by surfactant concentration and hydrodynamic-stretching sensitive to flow type. As macromolecules can undergo relatively large stretch, even coil-stretch transition, under the effect of an extensional flow, the extent of stretching determines the value of Tr especially in the finite extensibility regime. We find that Tr values for the P^0S^- systems are nearly a factor of 3 lower, implying the extensibility itself is 1.7

times lower, consistent with the previous determination of conformational changes in an uncharged polymer that interacts with an ionic surfactant. We anticipate that protocols and findings described herein will help in a better understanding of the rheological and processing behavior of formulations containing flexible uncharged polymers and ionic surfactants, especially during processing operations involving strong extensional flows.

Author Contributions

CM primarily carried out all the experiments described in the study. TM, under CM's mentorship, carried out the tensiometry experiments. CM and VS analyzed the data and wrote the manuscript.

Conflicts of interest

"There are no conflicts to declare".

Acknowledgements

CM and VS would like to acknowledge funding support by NSF CBET 1806011, PPG industries, and the 3M nontenured faculty award (NTFA). CM also wishes to acknowledge a Teaching Assistantship by the Department of Chemistry at UIC. TM is currently employed at Abbott (Gurnee, IL) and carried out research as an undergraduate student at UIC. The authors acknowledge Dr. Naveen Reddy (U. Hasselt), Dr. Hari Katepalli (Dow), and Dr. Karthika Suresh, a post-doctoral associate and the students from the ODES-lab for a close reading of the manuscript. Lastly, the authors wish to acknowledge discussions with Dr. J. Dinic (UChicago) on the influence of the underlying substrate for JD had carried out an evaluation of the influence of different substrates first at UIC and later at KU Leuven in collaboration with Dr. Naveen Reddy, Dr. Susanna Formenti, and Prof. Christian Clasen.

References

1. R. G. Larson, *The Structure and Rheology of Complex Fluids*, Oxford University Press, New York, 1999.
2. M. Rubinstein and R. H. Colby, *Polymer Physics*, Oxford Univ. Press: New York, 2003.
3. Z.-G. Wang, *Macromolecules*, 2017, **50**, 9073-9114.
4. M. Muthukumar, *Macromolecules*, 2017, **50**, 9828-9560.
5. J. R. Prakash, *Curr. Opin. Colloid Interface Sci.*, 2019, **43**, 63-79.
6. S. Srivastava and M. V. Tirrell, *Adv. Chem. Phys*, 2016, **161**, 499-544.
7. E. S. G. Shaqfeh, *AlChE J.*, 2019, **65**, e16575.
8. E. Guzmán, S. Llamas, A. Maestro, L. Fernández-Peña, A. Akanno, R. Miller, F. Ortega and R. G. Rubio, *Adv. Colloid Interface Sci.*, 2016, **233**, 38-64.
9. E. D. Goddard, *J. Colloid Interface Sci.*, 2002, **256**, 228-235.
10. E. D. Goddard and K. P. Ananthapadmanabhan, eds., *Interactions of Surfactants with Polymers and Proteins*, CRC press, 1993.
11. L. Piculell and B. Lindman, *Adv. Colloid Interface Sci.*, 1992, **41**, 149-178.
12. E. D. Goddard, *J. Am. Oil Chem. Soc.*, 1994, **71**, 1-16.
13. R. Nagarajan, *J. Chem. Phys.*, 1989, **90**, 1980-1994.
14. R. Nagarajan, In *Polymer-surfactant interactions*, New Horizons: Detergents for the New Millennium Conference Invited Paper, American Oil Chemists Society and Consumer Specialty Products Association, 2001.
15. T. L. Carlson, J. Y. Lock and R. L. Carrier, *Ann. Rev. Biomed. Eng.*, 2018, **20**, 197-220.
16. E. Hilz and A. W. P. Vermeer, *Crop Protection*, 2013, **44**, 75-83.
17. E. Villermaux, *J. Fluid Mech*, 2020, **898**, P1.
18. J. Kim, Y. Gao, C. Hebebrand, E. Peirtsegaele and M. E. Helgeson, *Soft Matter*, 2013, **9**, 6897-6910.
19. A. Jaishankar, V. Sharma and G. H. McKinley, *Soft Matter*, 2011, **7**, 7623-7634.
20. N. Kristen and R. von Klitzing, *Soft Matter*, 2010, **6**, 849-861.
21. A. Gupta, H. B. Eral, T. A. Hatton and P. S. Doyle, *Soft matter*, 2016, **12**, 2826-2841.
22. J. N. Israelachvili, *Intermolecular and Surface Forces*, Academic Press, 3rd edn., 2011.
23. E. D. Goddard, *Coll. Surf.*, 1986, **19**, 255-300.
24. B. Z. Shang, Z. Wang and R. G. Larson, *J. Phys. Chem. B*, 2008, **112**, 2888-2900.
25. J. Francois, J. Dayantis and J. Sabbadin, *Eur. Polym. J.*, 1985, **21**, 165-174.
26. S. Banerjee, C. Cazeneuve, N. Baghdadli, S. Ringeissen, F. A. M. Leermakers and G. S. Luengo, *Soft Matter*, 2015, **11**, 2504-2511.
27. L. Kunche and U. Natarajan, *Soft Matter*, 2021.
28. J. Eggers and M. A. Fontelos, *Singularities: Formation, Structure, and Propagation*, Cambridge University Press, Cambridge, UK, 2015.
29. G. H. McKinley, *Rheol. Rev.*, 2005, 1-48.
30. O. A. Basaran, H. Gao and P. P. Bhat, *Ann. Rev. Fluid. Mech.*, 2013, **45**, 85-113.
31. M. Abkarian and H. A. Stone, *Phys. Rev. Fluids*, 2020, **5**, 102301.
32. R. Hamed, D. M. Schenck and J. Fiegel, *Soft Matter*, 2020, **16**, 7823-7834.
33. B. E. Scharfman, A. H. Techet, J. W. M. Bush and L. Bourouiba, *Exp. Fluids*, 2016, **57**, 24.
34. Y. Christanti and L. M. Walker, *J. Non-Newtonian Fluid Mech.*, 2001, **100**, 9-26.
35. Y. Christanti and L. M. Walker, *J. Rheol.*, 2002, **46**, 733-748.
36. Y. Christanti and L. M. Walker, *Atomization Sprays*, 2006, **16**, 777-790.
37. V. Sharma, S. J. Haward, J. Serdy, B. Keshavarz, A. Soderlund, P. Threlfall-Holmes and G. H. McKinley, *Soft Matter*, 2015, **11**, 3251-3270.
38. B. Keshavarz, V. Sharma, E. C. Houze, M. R. Koerner, J. R. Moore, P. M. Cotts, P. Threlfall-Holmes and G. H. McKinley, *J. Non-Newtonian Fluid Mech.*, 2015, **222**, 171-189.
39. B. Keshavarz, E. C. Houze, J. R. Moore, M. R. Koerner and G. H. McKinley, *Phys. Rev. Lett.*, 2016, **117**, 154502.
40. V. M. Entov and E. J. Hinch, *J. Non-Newtonian Fluid Mech.*, 1997, **72**, 31-54.

41. V. M. Entov and A. L. Yarin, *Fluid Dyn.*, 1984, **19**, 21-29.
42. V. Tirtaatmadja, G. H. McKinley and J. J. Cooper-White, *Phys. Fluids*, 2006, **18**, 043101.
43. O. Arnolds, H. Buggisch, D. Sachsenheimer and N. Willenbacher, *Rheol. Acta*, 2010, **49**, 1207-1217.
44. J. Dinic, Y. Zhang, L. N. Jimenez and V. Sharma, *ACS Macro Lett.*, 2015, **4**, 804-808.
45. J. Dinic, M. Biagioli and V. Sharma, *J. Polym. Sci., Part B: Polym. Phys.*, 2017, **55**, 1692-1704.
46. J. Dinic, L. N. Jimenez and V. Sharma, *Lab Chip*, 2017, **17**, 460-473.
47. J. Dinic and V. Sharma, *Proc. Natl. Acad. Sci. U.S.A.*, 2019, **116**, 8766–8774.
48. J. Dinic and V. Sharma, *Macromolecules*, 2020, **53**, 4821-4835.
49. T. Q. Nguyen and H. H. Kausch, *Flexible Polymer Chains in Elongational Flow: Theory and Experiment*, Springer-Verlag, Berlin, 1999.
50. D. F. James and K. Walters, in *Techniques of Rheological Measurement*, ed. A. A. Collyer, Elsevier, New York, 1994, ch. 2, pp. 33-53.
51. L. E. Rodd, T. P. Scott, J. J. Cooper-White and G. H. McKinley, *Appl. Rheol.*, 2005, **15**, 12-27.
52. C. J. S. Petrie, *J. Non-Newtonian Fluid Mech.*, 2006, **137**, 1-14.
53. J. Dinic and V. Sharma, *Macromolecules*, 2020, **53**, 3424-3437.
54. P. Fischer and E. J. Windhab, *Curr. Opin. Colloid Interface Sci.*, 2011, **16**, 36-40.
55. C. W. Macosko, *Rheology: Principles, Measurements and Applications*, VCH Publishers Inc, New York, 1994.
56. J. R. Eastman, J. W. Goodwin and A. M. Howe, *Coll. Surf. A: Physicochem. Eng. Aspects*, 2000, **161**, 329-338.
57. L. M. Smitter, J. F. Guedez, A. J. Müller and A. E. Saez, *J. Colloid Interface Sci.*, 2001, **236**, 343-353.
58. L. M. Smitter, J. C. Ruiz, M. E. Torres, A. J. Müller and A. E. Saez, *J. Colloid Interface Sci.*, 2002, **251**, 388-397.
59. L. M. Smitter, M. E. Torres, A. J. Müller and A. E. Saez, *J. Colloid Interface Sci.*, 2001, **244**, 164-172.
60. J. J. Cooper-White, R. C. Crooks, K. Chockalingam and D. V. Boger, *Ind. Eng. Chem. Res.*, 2002, **41**, 6443-6459.
61. M. F. Torres, A. J. Muller, M. A. Szidarovszky and A. E. Saez, *J. Colloid Interface Sci.*, 2008, **326**, 254-260.
62. E. Miller and J. Cooper-White, *J. Non-Newtonian Fluid Mech.*, 2009, **160**, 22-30.
63. R. Wang, G. Dorr, A. Hewitt and J. Cooper-White, *Coll. Surf. A: Physicochem. Eng. Aspects*, 2016, **500**, 88-97.
64. P. Dontula, M. Pasquali, L. Scriven and C. W. Macosko, *Rheol. Acta*, 1997, **36**, 429-448.
65. L. Campo-Deano and C. Clasen, *J. Non-Newtonian Fluid Mech.*, 2010, **165**, 1688-1699.
66. L. N. Jimenez, J. Dinic, N. Parsi and V. Sharma, *Macromolecules*, 2018, **51**, 5191-5208.
67. L. N. Jimenez, C. D. V. Martínez Narváez and V. Sharma, *Phys. Fluids*, 2020, **32**, 012113.
68. L. N. Jimenez, C. D. M. Narváez, C. Xu, S. Bacchi and V. Sharma, *Soft Matter*, 2021, **in press**.
69. L. N. Jimenez, C. D. V. M. Narváez, C. Xu, S. Bacchi and V. Sharma, *Surface Science and Adhesion in Cosmetics*, 2021, 109-150.
70. K. W. Hsiao, J. Dinic, Y. Ren, V. Sharma and C. M. Schroeder, *Phys. Fluids*, 2017, **29**, 121603.
71. A. V. Walter, L. N. Jimenez, J. Dinic, V. Sharma and K. A. Erk, *Rheol. Acta*, 2019, **58**, 145-157.
72. K. A. Marshall, A. M. Liedtke, A. H. Todt and T. W. Walker, *Exp. Fluids*, 2017, **58:69**, 9.
73. N. S. Suteria, S. Gupta, R. Potineni, S. K. Baier and S. A. Vanapalli, *Rheol. Acta*, 2019, **58**, 403-417.
74. K. A. Marshall and T. W. Walker, *Rheol. Acta*, 2019, **58**, 573-590.
75. T. J. Murdoch, E. Pashkovski, R. Patterson, R. W. Carpick and D. Lee, *ACS Appl. Polym. Mater.*, 2020, **2**, 4062-4070.
76. Y. Su, B. Palacios and R. Zenit, *Phys. Rev. Fluids*, 2021, **6**, 033303.
77. A. Franco-Gómez, H. Onuki, Y. Yokoyama, Y. Nagatsu and Y. Tagawa, *Exp. Fluids*, 2021, **62**, 1-15.
78. S. Gupta and S. A. Vanapalli, *Phys. Fluids*, 2020, **32**, 012006.
79. M. Rosello, S. Sur, B. Barbet and J. P. Rothstein, *J. Non-Newtonian Fluid Mech.*, 2019, **266**, 160-170.
80. S. Khandavalli, N. Sharma-Nene, S. Kabir, S. Sur, J. P. Rothstein, K. C. Neyerlin, S. A. Mauger and M. Ulsh, *ACS Appl. Polym. Mater.*, 2021.
81. Y. Zhang and S. J. Muller, *Phys. Rev. Fluids*, 2018, **3**.
82. S. J. Wu and H. Mohammadigoushki, *J. Rheol.*, 2018, **62**, 1061-1069.
83. R. Omidvar, S. Wu and H. Mohammadigoushki, *J. Rheol.*, 2019, **63**, 33-44.
84. S. Wu and H. Mohammadigoushki, *Phys. Rev. Fluids*, 2020, **5**, 053303.
85. N. C. Christov, K. D. Danov, P. A. Kralchevsky, K. P. Ananthapadmanabhan and A. Lips, *Langmuir*, 2006, **22**, 7528-7542.
86. V. B. Fainerman, R. Miller and P. Joos, *Colloid. Polym. Sci.*, 1994, **272**, 731-739.
87. E. I. Franses, O. A. Basaran and C. H. Chang, *Curr. Opin. Colloid Inter. Sci.*, 1996, **1**, 296-303.
88. J. A. Odell, A. Keller and Y. Rabin, *J. Chem. Phys.*, 1988, **88**, 4022-4028.
89. S. Garrepally, S. Jouenne, P. D. Olmsted and F. Lequeux, *J. Rheol.*, 2020, **64**, 601-614.
90. C. Clasen, J. P. Plog, W. M. Kulicke, M. Owens, C. Macosko, L. E. Scriven, M. Verani and G. H. McKinley, *J. Rheol.*, 2006, **50**, 849-881.
91. A. J. Müller, Y. Garcés, M. Torres, B. Scharifker and A. E. Sáez, in *Aqueous Polymer—Cosolute Systems*, Springer, 2003, pp. 73-81.
92. B. Cabane, *J. Phys. Chem.*, 1977, **81**, 1639-1645.
93. B. Cabane and R. Duplessix, *J. Phys.*, 1982, **43**, 1529-1542.
94. B. Cabane and R. Duplessix, *Coll. Surf.*, 1985, **13**, 19-33.
95. B. Cabane and R. Duplessix, *J. Phys.*, 1987, **48**, 651-662.
96. K. Shirahama, K. Tsujii and T. Takagi, *J. Biochem.*, 1974, **75**, 309-319.
97. F. H. Quina, P. M. Nassar, J. B. S. Bonilha and B. L. Bales, *J. Phys. Chem.*, 1995, **99**, 17028-17031.
98. B. Cabane, R. Duplessix and T. Zemb, *J. Phys.*, 1985, **46**, 2161-2178.
99. P. G. de Gennes, F. Brochard-Wyart and D. Quéré, *Capillarity and Wetting Phenomena: Drops, Bubbles, Pearls, Waves*, Springer-Verlag, New York, 2004.
100. D. Bonn, J. Eggers, J. Indekeu, J. Meunier and E. Rolley, *Rev. Mod. Phys.*, 2009, **81**, 739-805.
101. S. Kumar, *Ann. Rev. Fluid. Mech.*, 2014, **47**, 67-94.
102. H. W. Kang, H. J. Sung, T.-M. Lee, D.-S. Kim and C.-J. Kim, *J. Micromechanics Microeng.*, 2008, **19**, 015025.

103. S. Dodds, M. Carvalho and S. Kumar, *Phys. Fluids*, 2011, **23**, 092101-092101-092111.
104. H. Chen, A. Amirfazli and T. Tang, *Langmuir*, 2013, **29**, 3310-3319.
105. A. K. Sankaran and J. P. Rothstein, *J. Non-Newtonian Fluid Mech.*, 2012, **175**, 64-75.
106. B. Qian and K. S. Breuer, *J. Fluid Mech.*, 2011, **666**, 554-572.
107. J. Dinic and V. Sharma, *Phys. Fluids*, 2019, **31**, 021211.
108. J. Zhou and M. Doi, *Phys. Rev. Fluids*, 2018, **3**, 084004.
109. A. Ardekani, V. Sharma and G. H. McKinley, *J. Fluid Mech.*, 2010, **665**, 46-56.
110. C. Wagner, L. Bourouiba and G. H. McKinley, *J. Non-Newtonian Fluid Mech.*, 2015, **218**, 53-61.
111. J. Eggers, M. A. Herrada and J. H. Snoeijer, *J. Fluid Mech.*, 2020, **887**.
112. A. Deblais, M. A. Herrada, J. Eggers and D. Bonn, *J. Fluid Mech.*, 2020, **904**.
113. P. P. Bhat, S. Appathurai, M. T. Harris, M. Pasquali, G. H. McKinley and O. A. Basaran, *Nature Phys.*, 2010, **6**, 625-631.
114. R. Prabhakar, S. Gadkari, T. Gopesh and M. J. Shaw, *J. Rheol.*, 2016, **60**, 345-366.
115. R. Prabhakar, C. Sasmal, D. A. Nguyen, T. Sridhar and J. R. Prakash, *Phys. Rev. Fluids*, 2017, **2**, 011301.
116. M. Renardy, *Rheology Rev.*, 2004, **2**, 171-196.
117. M. Stelter, G. Brenn, A. L. Yarin, R. P. Singh and F. Durst, *J. Rheol.*, 2000, **44**, 595-616.
118. M. Stelter, G. Brenn, A. L. Yarin, R. P. Singh and F. Durst, *J. Rheol.*, 2002, **46**, 507-527.
119. F. Jin, N. R. Gupta and K. J. Stebe, *Phys. Fluids*, 2006, **18**, 022103.
120. M. R. de Saint Vincent, J. Petit, M. Aytouna, J.-P. Delville, D. Bonn and H. Kellay, *J. Fluid Mech.*, 2012, **692**, 499-510.
121. M. Roché, M. Aytouna, D. Bonn and H. Kellay, *Phys. Rev. Lett.*, 2009, **103**, 264501.
122. W. Lee, L. M. Walker and S. L. Anna, *Macromolecular Mater. Eng.*, 2011, **296**, 203-213.
123. M.-L. E. Timmermans and J. R. Lister, *J. Fluid Mech.*, 2002, **459**, 289-306.
124. P. M. Kamat, B. W. Wagoner, S. S. Thete and O. A. Basaran, *Phys. Rev. Fluids*, 2018, **3**, 043602.
125. D. Sachsenheimer, B. Hochstein and N. Willenbacher, *Rheol. Acta*, 2014, **53**, 725-739.
126. N. Willenbacher, Y. Matter, I. Gubaydullin and V. Schaedler, *Korea-Australia Rheol. J.*, 2008, **20**, 109-116.
127. B. Yesilata, C. Clasen and G. H. McKinley, *J. Non-Newtonian Fluid Mech.*, 2006, **133**, 73-90.
128. A. Bhardwaj, E. Miller and J. P. Rothstein, *J. Rheol.*, 2007, **51**, 693-719.
129. D. Sachsenheimer, C. Oelschlaeger, S. Müller, J. Küstner, S. Bindgen and N. Willenbacher, *J. Rheol.*, 2014, **58**, 2017-2042.
130. R. Omidvar, A. Dalili, A. Mir and H. Mohammadigoushki, *J. Non-Newtonian Fluid Mech.*, 2018, **252**, 48-56.
131. H. Tan, K. C. Tam, V. Tirtaatmadja, R. D. Jenkins and D. R. Bassett, *J. Non-Newtonian Fluid Mech.*, 2000, **92**, 167-185.